Proceedings of the ASME 2018 International Design Engineering Technical Conferences & Computers and Information in Engineering Conference
IDETC/CIE 2018
August 26-29, 2018, Quebec City, Canada

DETC2018-85620

SURROGATE BASED MULTI-OBJECTIVE OPTIMIZATION OF J-TYPE BATTERY THERMAL MANAGEMENT SYSTEM

Yuanzhi Liu*
The University of Texas at Dallas
Richardson, TX 75080
Email: yuanzhi.liu@utdallas.edu

Payam Ghassemi*
University at Buffalo
Buffalo, NY, 14260
Email: payamgha@buffalo.edu

Souma Chowdhury†
University at Buffalo
Buffalo, NY 14260
Email: soumacho@buffalo.edu

Jie Zhang‡
The University of Texas at Dallas
Richardson, TX 75080
Email: jiezhang@utdallas.edu

ABSTRACT

This paper proposes a novel and flexible J-type air-based battery thermal management system (BTMS), by integrating conventional Z-type and U-type BTMS. With two controlling valves, the J-type BTMS can be adaptively controlled in real time to help balance the temperature uniformity and energy efficiency under various charging/discharging situations (especially extreme fast changing). Results of computational fluid dynamics simulations show that the J-type system performs better than the U-type and Z-type systems. To further improve the thermal performance of the proposed J-type BTMS, a surrogate-based multi-objective optimization is performed, with the consideration of the two major objectives, i.e., uniformity and energy efficiency. The concurrent surrogate selection (COSMOS) framework is adopted in this paper to determine the most suitable surrogate models. Optimization results show that: (i) the uniformity of the temperature distribution is improved by 38.6% compared to the benchmark, (ii) the maximum temperature is reduced by 19.1%, and (iii) the pressure drop is decreased by 14.5%.

Keywords: Battery thermal management, surrogate modeling, multi-objective optimization, electrical vehicle

1 INTRODUCTION

Electric vehicles (EVs) are likely to flourish in the near future after a rapid development in the past few years. Several major automobile manufacturers have added EVs into their short-term portfolio as a response of the growing movements to cut down vehicle emissions. As the only energy source, in retrospect, the battery technologies that are utilized in EV industry have progressed from low energy density like lead-acid battery, nickel-cadmium battery, to high energy density like lithium-ion battery. The emergence of lithium-ion battery has promoted the rapid development of EVs. Lithium-ion battery is currently one of the most widely used batteries in EVs due to its excellent properties, such as high energy density, low self-charging, and low main-

*Ph.D. Student, Department of Mechanical Engineering, ASME Student Member.

†Assistant Professor, Department of Mechanical and Aerospace Engineering, ASME Professional Member.

‡Assistant Professor, Department of Mechanical Engineering, ASME Professional Member. Address all correspondence to this author.

tenance. However, potential issues, i.e. safety and aging effects, might still challenge its wide application in EVs. It has been known that the operating temperature has a significant impact on the performance and health of lithium batteries. The optimum temperature should be well controlled in a narrow range, i.e., 15-35 °C [1], 25-45 °C [2],and 20-45 °C [3] as reported in the literature. Otherwise, thermal runaway may accelerate the electrode degradation and capacity deduction or even safety issues like fire and explosion, especially under extreme fast charging (XFC) situations. Therefore, A battery thermal management system (BTMS) is necessary to maintain thermal surroundings, thereby preventing potential safety risks.

1.1 Literature Review of BTMS

A significant amount of work has been conducted in the literature on the design and evaluation of battery thermal management systems. State-of-the-art BTMS includes forced liquid cooling, forced air cooling, heat pipe, phase change material (PCM), and a hybrid approach of those technologies. Most of existing work has emphasized the cooling aspect, while the study of heating aspect was rarely reported.

Compared with other thermal management systems, air-based BTMS has been widely employed in industry due to its remarkable advantages like light weight, simple structure, and low cost. For example, Nissan Leaf [4] with passive pure air cooling has successfully updated to its second generation and the air cooling system has proved to be reliable. The majority of the existing work in air-based BTMS focuses on cooling channel design and optimization. For example, Park [5] proposed and compared a Z-type and a U-type air-based BTMS with simulations, and found that the thermal requirement can be achieved by changing the tapered manifold and pressure for both types. Xun et al. [6] investigated the internal temperature distribution of battery cells with computational fluid dynamics (CFD) simulations, and suggested that changing the counter flow arrangement and direction periodically may improve the thermal performance. Shahid et al. [7] examined the effectiveness of multiple vortex generators with experiments, and results showed that both the maximum temperature and uniformity could be improved. Wang et al. [8] proposed to use a surrogate based multidisciplinary optimization method to optimize the design of air-based BTMS, thereby improving the battery lifetime.

A liquid cooling system employs a closed liquid circulation with a higher thermal capacity, making the heat dissipation more effective, and meanwhile adding considerable extra weight to the whole system due to its complicated ancillary components like pipe, pump, and coolant. Several types of micro channel [9] or thin plate [10, 11] structure coupled with various kinds of coolant and heat sink have been investigated in previous studies. For example, Zhao et al. [12] proposed a mini-channel liquid cooling structure for a cylindrical battery pack, and the results showed it could control the temperature with 40°C under a $5C$ discharging situation. Wang et al. [13] investigated the cooling effectiveness of using cylindrical tubes with silica saturated in between the prismatic batteries, and summarized the coolant flow rates for different charging situations. Jin et al. [14] designed a novel liquid cold plate with simple oblique fins at their optimum angle and width, and experimental results showed that the thermal performance was better than the conventional liquid based BTMS. Recently it tends to shift the foci of interest in liquid cooling research from surface cooling to tab cooling, which has been reported to be more efficient [15, 16].

A pure PCM cooling system generally utilizes PCM as a heat absorption buffer and final heat sink. The dissipation capacity of a PCM cooling system depends on the properties of PCM, such as specific heat capacity and mass[17, 18, 19]. A hybrid PCM cooling system cooperates with air or liquid cooling to transfer the heat to the ambient environment[20, 21]. It was reported that the hybrid PCM system can yield a higher efficiency than pure PCM or forced convective cooling, especially after a long time operation [22]. Similarly, heat pipe cooling could also be broadly divided into two categories: pure heat pipe [23] and hybrid heat pipe [24] based cooling. A hybrid heat pipe cooling couples with fan ventilation can effectively control the temperature evenly under abusive discharging conditions [22].

1.2 Research Motivation and Objective

All the cooling technologies discussed above have already been proven to have the capability to well control the battery temperature in an appropriate range. Among different types of BTMS, air cooling has incomparable advantages in terms of weight and power-to-weight ratio. Moreover, the approaching air can be drawn into the battery pack without energy consumption when driving. There are two major types of air-based BTMS: Z-type and U-type. Existing air cooling systems attempt to rearrange the Z-type and U-type channel size to enable uniform air flow rate distribution with a lower pressure drop, and hence to lower the maximum temperature and improve the uniformity among battery cells energy efficiently. It is generally challenging to maintain the trade-off between temperature uniformity and energy efficiency for huge battery packs, especially under XFC situations. To address this challenge, this paper proposes a novel and flexible air cooling structure called J-type, which is based on the existing Z-type and U-

type. With two controlling valves, the J-type BTMS can be adaptively controlled in real time to help balance the temperature uniformity and energy efficiency. The J-type BTMS can also switch to Z-type or U-type by completely closing one of the two controlling valves.

To further improve the performance of the proposed J-type BTMS, a multi-objective optimization is performed, with the consideration of the two major objectives (i.e., uniformity and energy efficiency). First, a CFD model of the J-type BTMS is built using ANSYS FLUENT. In order to effectively conduct optimization, surrogate models are constructed to represent the objectives and constraints as functions of design variables, i.e., battery cell passaging spacing sizes, inlet and outlet manifold sizes, and mass flow rate of the cooling air. The concurrent surrogate selection (COSMOS) framework is adopted in this paper to determine the most suitable surrogate models.

The remainder of the paper is organized as follows. First, BTMS modeling is developed in the next section, with a detailed comparison among J-, Z-, and U-type BTMS. Then, surrogate-based multi-objective optimization is performed and BTMS optimal results are discussed. Concluding remarks and future work are discussed in the last section.

2 BTMS MODELING

2.1 Conceptual Design of J-type Cooling System

By taking the advantages of both U-type and Z-type air-based BTMS, a novel system named J-type is proposed in this paper. A conceptual design of the J-type BTMS is illustrated in Fig. 1. The battery pack in the prototype consists of ten battery cells, and the size of each cell is set to be 151 mm in height, 65 mm in length, and 16 mm in width. The size of the battery cell is selected according to Ref. [5].

Generally, a higher charging/discharging rate requires a larger air flow rate to take away the heat, which may also lead to discrepancies in the distribution of flow among different cells. Thus, the topology of battery cells in a pack is critically important, which needs to be designed with an optimal layout. In addition, under different operation conditions (i.e., XFC, normal charging, and discharging), the configuration of the proposed J-type BTMS is expected to be adaptively controlled, by changing air flow rate and the inlet/outlet manifold sizes to ensure that the system operates at an optimal status. As illustrated in Fig.1, the sizes of passages and the inlet manifold will be optimized and fixed by considering multiple distinct operating conditions, while the air flow rate and the two values at the outlet (U and Z) will be adaptively controlled in real time. The hypothesis of this J-type BTMS design is that the thermal

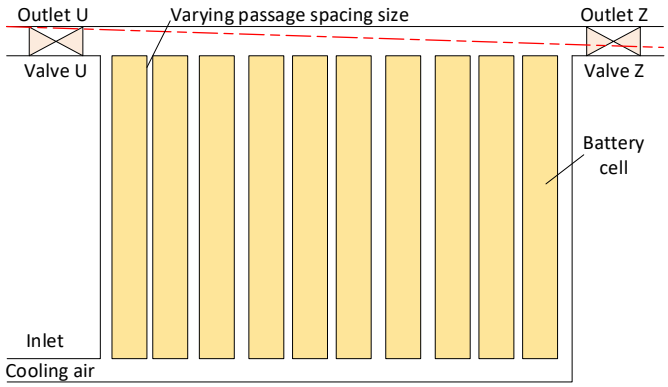

FIGURE 1. The conceptual design of a J-type air-based BTMS

performance can be improved by adaptively changing the air flow field via controlling the valves' opening degree at the outlet.

The whole battery module can be maintained in a standard shape, no matter in which direction the new layers of the battery cells are added. Assembling multiple uniform modules can form a large-scale and compact battery system, which provides the advantages such as high volumetric energy density and large flexibility for the whole vehicle arrangement [22].

2.2 CFD Modeling of J-type Cooling System

A three-dimensional (3D) CFD simulation model is built in ANSYS FLUENT with the k-ϵ turbulence model. The total size of the model converged to 1,800,000 elements after a grid dependence analysis. Mass flow rate is chosen as the inlet boundary condition while pressure outlet is selected as the outlet boundary condition. Only the heat transfer between the battery cells and cooling air is considered during the calculation. The battery cell in the model is assumed to be a uniform heat source with an equivalent volumetric heat generation rate of 62.5 W/L, corresponding to a 3 A fast charging operation condition based on the work of Bandhauer et al. [25] and FernÃąndez et al. [26].

A benchmark model with an even 3 mm passage spacing size, an equal 8 mm inlet/outlet manifold size, and an initial inlet mass flow rate 7.1 g/s is set up for comparison among the $J-$, $Z-$, and $U-$type BTMS. The J-type outlet structure could be simplified into a tapered manifold, as indicated by the dashed red line in Fig. 1. Similarly, CFD simulation models of the Z-type and $U-type$ systems are also built with the same settings. The simulations take approximately 15 minutes to converge using a six-core workstation.

2.3 Validation of J-Type Cooling System

Figure 2 shows the sandwich-like temperature distributions of U-type, Z-type, and J-type BTMS with steady state simulation results. It is seen from Fig. 2(a) that temperature of the rear cells are much higher than those of the front ones with the U-type BTMS, while the Z-type battery cells' temperature in Fig. 2(b) are distributed in an opposite way. The maximum temperature and temperature difference of both the U and Z types are approximately the same, i.e., close to 22 K, which is relatively high under the selected benchmark operation condition. The thermal performance of the J-type BTMS is significantly better than that of the U and Z types, which results in a maximum temperature rise of 11.3 K and a temperature difference of 6.3 K. The J-type also performs well in terms of pressure drop, as shown in Table. 1.

TABLE 1. Comparing three types of BTMS

Evaluation Index	U-type	Z-type	J-type
T_{max}(K)	322.3	323.5	311.5
ΔT(K)	18.2	20.1	6.3
$\Delta P(Pa)$	406.1	356.4	199.4

T_{max}: maximum temperature ΔT: maximum temperature difference
ΔP: Pressure drop

Previous studies [22, 27] have shown that both the maximum temperature and the temperature difference among cells will increase significantly when a larger heat source is added, such as under XFC conditions. Thus, the proposed J-type BTMS is expected to provide more significant advantages over the conventional U-type and Z-type BTMS, especially facing fast charging/discharging conditions.

3 SURROGATE MODELING AND OPTIMIZATION

3.1 Surrogate Model Selection

Given the availability of characteristically diverse well-known surrogate modeling techniques, e.g., Quadratic Response Surfaces (QRS) [28], Moving Least Square [29], Radial Basis Functions (RBF) [30], Kriging [31], Support Vector Regression (SVR) [32], Artificial Neural Networks (ANN), and Sparse polynomial chaos expansions [33, 34], the selection of the most suitable surrogate model for practical problems or data sets (such as our BTMS design) is far from intuitive. This challenge has led to the development of automated model selection frameworks over the past two decades [35, 36, 37, 38, 39, 40, 41, 42, 43, 44]. In this paper, we exploit our recently developed model selection framework called Concurrent surrogate Model Selection or COSMOS [44, 45, 46], which unlike most other existing methods coherently operates at all the three levels of variation across models choices, namely: 1) selecting the model type, 2) selecting the kernel function type, and (3) determining the optimal values of the typically user-prescribed parameters. The latter can be called hyper-parameters, in order to differentiate them from parameters that are typically determined during the model training process. The optimal model selection in COSMOS is driven by measures of model error or model uncertainty that serves as the selection criteria. These model error measures are computed by the Predictive Estimation of Model Fidelity(PEMF) approach [47], which can be perceived as a robust sequential implementation of k-fold cross-validation. The candidate model types available for selection under COSMOS include Kriging (DACE implementation [48]), RBF, SVR (LIBSVM implementation [49]), and multi-layer-perceptron ANN (MATLAB's NN toolbox). More information regarding the model-kernel choices and bounds of hyper-parameter values can be found in [44].

Here, we need to construct four surrogate models, respectively representing the maximum in cell temperature or T_{max}, standard deviation in temperature increase across the cells or T_σ(Eq.1), the average temperature across cells or T_{avg}, and the pressure drop between the inlet and outlet or ΔP. The surrogate models will be mapping these four outputs to the following 15 parameters: i) the 11 inter-cell spacing parameters, $x_1 - x_{11}$, ii) the inlet manifold size, b_1, iii) the size of the two outlets b_2, b_3, and iv) the incoming mass flow rate, $\dot{m}$. The optimal surrogate models determined by COSMOS, and their predicted median error measures, are summarized in Table 2.

TABLE 2. Optimal surrogate models determined by COSMOS

Output	Model (Kernel)	HP	RAE
T_{avg}	Neural Network (MLP)	5	2.00e-3
T_{max}	Kriging (Exponential)	0.562	5.10e-3
T_σ	Neural Network (MLP)	3	4.28e-2
ΔP	Neural Network (MLP)	5	8.70e-2

RAE: relative absolute error HP: Hyper-parameter

$$T_\sigma = \sqrt{\frac{1}{N-1}\sum_{i=1}^{N}(\Delta T_i - \overline{\Delta T})^2} \quad (1)$$

where ΔT_i represents the maximum temperature rise on the battery surface, and $\overline{\Delta T}$ represents the average maximum temperature rise among the battery pack.

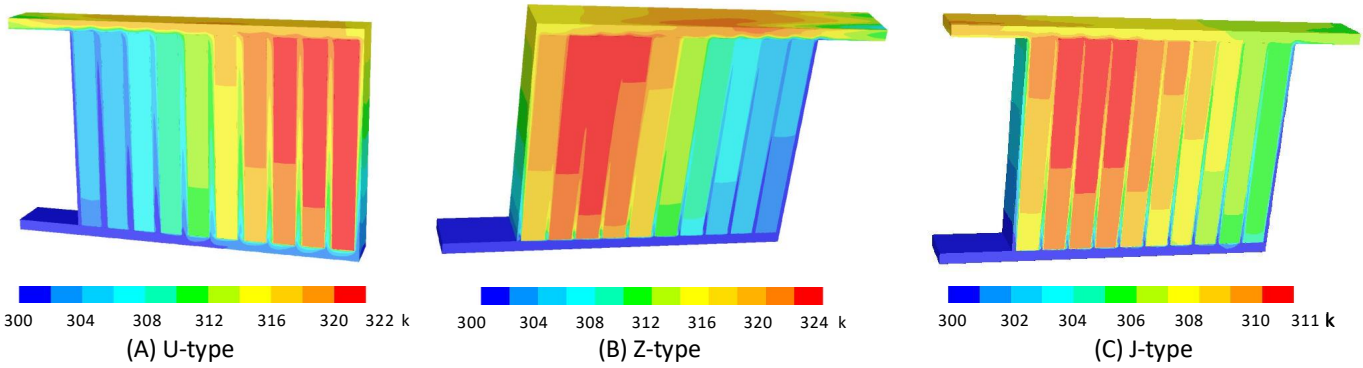

FIGURE 2. Temperature distributions of different types of air-based BTMS under 3 A fast charging operation condition

Here, the two important quantities of interest, used later in surrogate based optimization of the BTMS, are the temperature standard deviation across cells (T_σ) and the pressure drop (ΔP). Based on a correlation analysis among all input and output parameters and further numerical experiments, it was found that using the surrogate model estimates of T_{max} and T_{avg} as additional inputs to the surrogate models for the two primary quantities of interest (T_σ and ΔP), can lead to more reliable prediction of the latter. This hybrid model construction is illustrated in Fig. 3.

3.2 Surrogate-based Optimization

The multi-objective optimization of the J-type BTMS is formulated as:

$$\begin{cases} \text{find} & \mathbf{X} = [x_1, x_2, \cdots, x_{11}, b_1, b_2, b_3, \dot{m}] \\ \text{min} & \mathbf{f} = [T_\sigma, \Delta P] \\ \text{s.t.} & V = (\sum_{i=1}^{11} +160) \times (151 + b_1 + (b_2 + b_3)/2) \leq 36312 \\ & 300 \leq T_{max} \leq 318 \\ & 0.8 \leq x_i \leq 4.8 \quad (i = 1, 2, 3, \cdots, 11) \\ & 4 \leq b_1 \leq 14 \\ & 0.5 \leq b_j \leq 20.5 \quad (j = 2, 3) \\ & 3 \leq \dot{m} \leq 11 \end{cases} \tag{2}$$

where $\mathbf{X}$ represents the 15 input design parameters, including 11 inter-cell spacing sizes, x_i (mm), inlet manifold size, b_1 (mm), two outlet manifold sizes, b_2 (mm) and b_3 (mm), and mass flow rate of the incoming air, $\dot{m}$ (g/s). The optimization objective $\mathbf{f}$ consists of two objectives, i.e., the standard deviation in temperature across all battery cells, T_σ, and the pressure drop between the inlet and outlet, $\Delta P(Pa)$. The constraint of V represents the volume of the battery module; T_{max} is the maximum battery cell temperature, with an upper bound of 318 K [2, 3] and a lower bound of ambient temperature.

We take a (multi-step) sequential surrogate-based optimization approach, where the Pareto optimal results from each optimization are used to perform sequential sampling and updating of the surrogate models; the updated surrogate models are then again used for optimization. Here, we repeated this process two times.

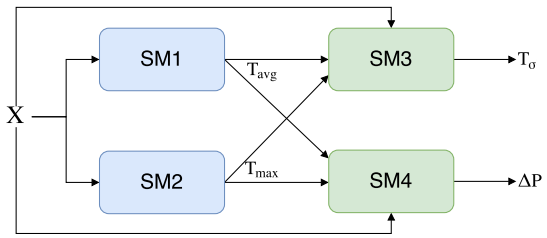

FIGURE 3. Hybrid model construction; SM stands for surrogate model.

3.3 Optimization Results

Figure 4 shows both the initial samples used for constructing the surrogate models (via COSMOS), as well as the Pareto optimal results obtained during the two optimization runs. All values shown here correspond to those estimated by the CFD model (and not the surrogate models), in order to allow fair comparisons. The final global Pareto frontier can be considered to be comprised of both a few initial samples as well as portions of Pareto set obtained by the two optimizations. It is also interesting to note that the re-sampling allowed the second optimization run to find a wider spread of Pareto solutions. However, given the presence of initial samples in the global Pareto front, this may not necessarily represent converged results,

TABLE 3. Excerpts of the optimal results

Case	x_1	x_2	x_3	x_4	x_5	x_6	x_7	x_8	x_9	x_{10}	x_{11}	b_1	b_2	b_3	$\dot{m}$	T_{max}	T_{σ^2}	ΔP
C0	3.0	3.0	3.0	3.0	3.0	3.0	3.0	3.0	3.0	3.0	3.0	8.0	8.0	8.0	7.1	311.5	1.4	199.6
C1	1.2	3.3	2.9	1.9	3.7	2.0	3.2	2.2	3.0	4.5	1.7	9.8	15.8	7.1	8.5	309.4	1.1	203.8
C2	0.8	4.0	2.3	1.9	4.8	2.0	4.8	1.7	2.9	4.8	4.6	9.9	5.5	10.3	10	318.3	3.4	143.9
C3	1.0	4.1	1.8	1.9	4.8	2.2	4.6	1.7	2.4	4.8	3.6	10.5	7.1	8.9	8.4	316.2	2.7	139.1
C4	1.4	3.2	2.2	1.9	2.1	1.8	2.4	1.3	3.4	1.5	1.4	12.3	11.9	12.6	7.6	308.9	0.8	190.1

C0: The benchmark case C1-C4: The optimal cases on the Pareto frontier

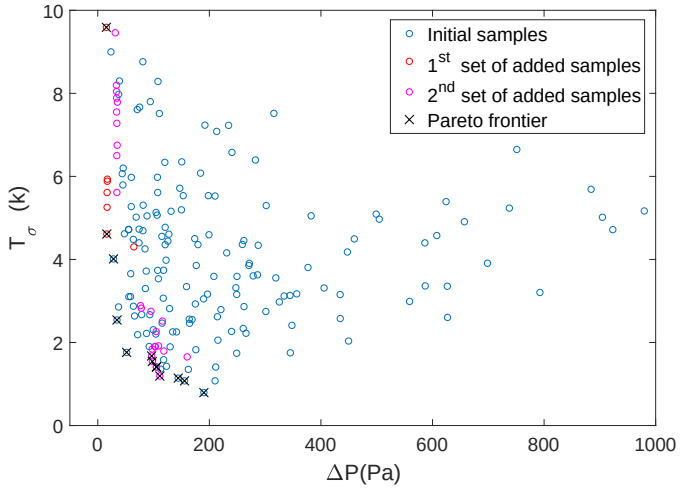

FIGURE 4. Initial samples and Pareto optimal points from surrogate-based multi-objective optimization

or might be affected by the level of error in the surrogate models. Further investigation is needed in the future to understand these issues, accomplish better converged results. Next, we discuss the validation and further physical analysis of the Pareto solutions with the high-fidelity thermal simulation.

The details of several optimal cases are listed in Table 3. Case 1 and Case 4 are better than the benchmark case in terms of both the evaluation index of T_{max} and T_σ, while Case 2 and Case 3 have advantages over the benchmark case on the pressure drop, ΔP. Case 4 is the only case that maintains absolute predominance over the benchmark case with a slightly higher flow rate. A CFD simulation of Case 4 with the same mass flow rate as the benchmark is then conducted for validation, as showed in Fig. 5.

Compared with Fig. 2, the temperature distribution of the optimal case is more uniform, with a standard deviation of 0.86 K, i.e., 38.6 % improvement compared to the benchmark. The maximum temperature is 309.3 K, and its correspondent temperature rise is 19.1 % lower compared to the benchmark. Moreover, the pressure drop decreases by 14.5%, from 199.6 Pa to 171.7 Pa. Overall, the surrogate-based optimization has effectively improved the thermal performance of the J-type air-based battery thermal management system.

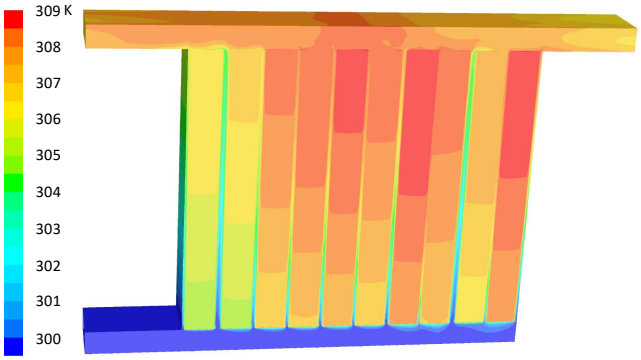

FIGURE 5. Temperature distribution of Case 4 for validation

4 CONCLUSION

A novel J-type BTMS was proposed and optimized in this paper. The performance of the J-type, U-type, and Z-type BTMS was compared, by analyzing the maximum temperature, the temperature difference, and the pressure drop between the inlet and outlet. It was found that the J-type system performed better than the U-type and Z-type systems.

To further improve the performance of the proposed J-type BTMS, a surrogate-based multi-objective optimization was performed, with the consideration of two major objectives, i.e., uniformity and energy efficiency. Optimization

results showed that: (i) the uniformity of the temperature distribution is improved by 38.6% compared to the benchmark, (ii) the maximum temperature is reduced by 19.1%, and (iii) the pressure drop is decreased by 14.5%.

Experimental evaluation and validation of the proposed J-type BTMS will be performed in the future.

REFERENCES

[1] Pesaran, A., Santhanagopalan, S., and Kim, G., 2013. Addressing the impact of temperature extremes on large format li-ion batteries for vehicle applications (presentation). Tech. rep., National Renewable Energy Lab.(NREL), Golden, CO (United States).

[2] Ramadass, P., Haran, B., White, R., and Popov, B. N., 2002. "Capacity fade of sony 18650 cells cycled at elevated temperatures: Part i. cycling performance". *Journal of Power Sources,* ***112***(2), pp. 606–613.

[3] Park, C., and Jaura, A. K., 2003. Dynamic thermal model of li-ion battery for predictive behavior in hybrid and fuel cell vehicles. Tech. rep., SAE Technical Paper.

[4] Hayes, J. G., and Davis, K., 2014. "Simplified electric vehicle powertrain model for range and energy consumption based on epa coast-down parameters and test validation by argonne national lab data on the nissan leaf". In Transportation Electrification Conference and Expo (ITEC), 2014 IEEE, IEEE, pp. 1–6.

[5] Park, H., 2013. "A design of air flow configuration for cooling lithium ion battery in hybrid electric vehicles". *Journal of power sources,* ***239***, pp. 30–36.

[6] Xun, J., Liu, R., and Jiao, K., 2013. "Numerical and analytical modeling of lithium ion battery thermal behaviors with different cooling designs". *Journal of Power Sources,* ***233***, pp. 47–61.

[7] Shahid, S., and Agelin-Chaab, M., 2017. "Analysis of cooling effectiveness and temperature uniformity in a battery pack for cylindrical batteries". *Energies,* ***10***(8), p. 1157.

[8] Wang, X., Li, M., Liu, Y., Sun, W., Song, X., and Zhang, J., 2017. "Surrogate based multidisciplinary design optimization of lithium-ion battery thermal management system in electric vehicles". *Structural and Multidisciplinary Optimization,* ***56***(6), pp. 1555–1570.

[9] Huo, Y., Rao, Z., Liu, X., and Zhao, J., 2015. "Investigation of power battery thermal management by using mini-channel cold plate". *Energy Conversion and Management,* ***89***, pp. 387–395.

[10] Panchal, S., Khasow, R., Dincer, I., Agelin-Chaab, M., Fraser, R., and Fowler, M., 2017. "Thermal design and simulation of mini-channel cold plate for water cooled large sized prismatic lithium-ion battery". *Applied Thermal Engineering,* ***122***, pp. 80–90.

[11] Putra, N., Ariantara, B., and Pamungkas, R. A., 2016. "Experimental investigation on performance of lithium-ion battery thermal management system using flat plate loop heat pipe for electric vehicle application". *Applied Thermal Engineering,* ***99***, pp. 784–789.

[12] Zhao, J., Rao, Z., and Li, Y., 2015. "Thermal performance of mini-channel liquid cooled cylinder based battery thermal management for cylindrical lithium-ion power battery". *Energy Conversion and Management,* ***103***, pp. 157–165.

[13] Wang, C., Zhang, G., Meng, L., Li, X., Situ, W., Lv, Y., and Rao, M., 2017. "Liquid cooling based on thermal silica plate for battery thermal management system". *International Journal of Energy Research,* ***41***(15), pp. 2468–2479.

[14] Jin, L., Lee, P., Kong, X., Fan, Y., and Chou, S., 2014. "Ultra-thin minichannel lcp for ev battery thermal management". *Applied Energy,* ***113***, pp. 1786–1794.

[15] Offer, G. J., Hunt, I., Merla, Y., Zhao, Y., von Srbik, M.-T., Marinescu, M., Yufit, V., Wu, B., Martinez-Botas, R., and Brandon, N. P., 2016. "Detecting, diagnosing and controlling degradation in lithium ion battery packs". In Meeting Abstracts, no. 2, The Electrochemical Society, pp. 1196–1196.

[16] Hunt, I. A., Zhao, Y., Patel, Y., and Offer, G., 2016. "Surface cooling causes accelerated degradation compared to tab cooling for lithium-ion pouch cells". *Journal of The Electrochemical Society,* ***163***(9), pp. A1846–A1852.

[17] Duan, X., and Naterer, G., 2010. "Heat transfer in phase change materials for thermal management of electric vehicle battery modules". *International Journal of Heat and Mass Transfer,* ***53***(23-24), pp. 5176–5182.

[18] Khateeb, S. A., Farid, M. M., Selman, J. R., and Al-Hallaj, S., 2004. "Design and simulation of a lithium-ion battery with a phase change material thermal management system for an electric scooter". *Journal of Power Sources,* ***128***(2), pp. 292–307.

[19] Lazrak, A., Fourmigué, J.-F., and Robin, J.-F., 2018. "An innovative practical battery thermal management system based on phase change materials: Numerical and experimental investigations". *Applied Thermal Engineering,* ***128***, pp. 20–32.

[20] Ling, Z., Wang, F., Fang, X., Gao, X., and Zhang, Z., 2015. "A hybrid thermal management system for lithium ion batteries combining phase change materials with forced-air cooling". *Applied energy,* ***148***, pp. 403–409.

[21] Zhao, R., Gu, J., and Liu, J., 2015. "An experimental study of heat pipe thermal management system with wet cooling method for lithium ion batteries". *Journal*

of Power Sources, ***273***, pp. 1089–1097.

[22] Zhao, R., Zhang, S., Liu, J., and Gu, J., 2015. "A review of thermal performance improving methods of lithium ion battery: electrode modification and thermal management system". *Journal of Power Sources,* ***299***, pp. 557–577.

[23] Greco, A., Cao, D., Jiang, X., and Yang, H., 2014. "A theoretical and computational study of lithium-ion battery thermal management for electric vehicles using heat pipes". *Journal of Power Sources,* ***257***, pp. 344–355.

[24] Burban, G., Ayel, V., Alexandre, A., Lagonotte, P., Bertin, Y., and Romestant, C., 2013. "Experimental investigation of a pulsating heat pipe for hybrid vehicle applications". *Applied Thermal Engineering,* ***50***(1), pp. 94–103.

[25] Bandhauer, T. M., Garimella, S., and Fuller, T. F., 2014. "Temperature-dependent electrochemical heat generation in a commercial lithium-ion battery". *Journal of Power Sources,* ***247***, pp. 618–628.

[26] García Fernández, V. M., Blanco Viejo, C., Anseán González, D., González Vega, M., Fernández Pulido, Y., and Alvarez Antón, J. C., 2016. "Thermal analysis of a fast charging technique for a high power lithium-ion cell". *Batteries,* ***2***(4), p. 32.

[27] Liu, Y., Li, M., and Zhang, J., 2017. "An experimental parametric study of air-based battery thermal management system for electric vehicles". In ASME 2017 International Design Engineering Technical Conferences and Computers and Information in Engineering Conference, American Society of Mechanical Engineers, pp. V02AT03A024–V02AT03A024.

[28] Qudeiri, J. E. A., Khadra, F. Y. A., Umer, U., and Hussein, H. M. A., 2015. "Response surface metamodel to predict springback in sheet metal air bending process". *International Journal of Materials, Mechanics and Manufacturing,* ***3***(4), pp. 203–224.

[29] Reute, I. M., Mailach, V. R., Becker, K. H., Fischersworring-Bunk, A., Schlums, H., and Ivankovic, M., 2017. "Moving least squares metamodels-hyperparameter, variable reduction and model selection". *In 14th International Probabilistic Workshop-Springer International Publishing*, pp. 63–80.

[30] Hardy, R. L., 1971. "Multiquadric equations of topography and other irregular surfaces". *Journal of Geophysical Research,* ***76***, pp. 1905–1915.

[31] Cressie, N., 1993. *Statistics for Spatial Data.* Wiley, New York.

[32] Basak, D., Srimanta, P., and Patranabis, D. C., 2007. "Support vector regression". *Neural Information Processing-Letters and Review,* ***11***(10), pp. 203–224.

[33] Blatman, G., and Sudret, B., 2011. "Adaptive sparse polynomial chaos expansion based on least angle regression". *Journal of Computational Physics,* ***230***(6), pp. 2345–2367.

[34] Jakeman, J. D., Narayan, A., and Zhou, T., 2017. "A generalized sampling and preconditioning scheme for sparse approximation of polynomial chaos expansions". *SIAM Journal on Scientific Computing,* ***39***(3), pp. A1114ÃćÂĂÂŞ–A1144.

[35] Jin, R., Chen, W., and Simpson, T. W., 2001. "Comparative studies of metamodelling techniques under multiple modelling criteria". *Structural and Multidisciplinary Optimization,* ***23***(1), pp. 1–13.

[36] Chen, P. W., Wang, J. Y., and Lee, H. M., 2004. "Model selection of svms using ga approach". In Neural Networks, 2004. Proceedings. 2004 IEEE International Joint Conference on, Vol. 3, IEEE, pp. 2035–2040.

[37] Fang, A., Rais-Rohani, M., Liu, Z., and Horstemeyer, M. F., 2005. "A comparative study of metamodeling methods for multiobjective crashworthiness optimization". *Computers & structures,* ***83***(25), pp. 2121–2136.

[38] Martin, J. D., and Simpson, T. W., 2005. "Use of kriging models to approximate deterministic computer models". *AIAA journal,* ***43***(4), pp. 853–863.

[39] Goel, T., and Stander, N., 2009. "Comparing three error criteria for selecting radial basis function network topology". *Computer Methods in Applied Mechanics and Engineering,* ***198***, pp. 2137–2150.

[40] Gorissen, D., Dhaene, T., and Turck, F. D., 2009. "Evolutionary model type selection for global surrogate modeling". *Journal of Machine Learning Research,* ***10***, pp. 2039–2078.

[41] Li, Y. F., Ng, S. H., Xie, M., and Goh, T. N., 2010. "A systematic comparison of metamodeling techniques for simulation optimization in decision support systems". *Applied Soft Computing,* ***10***(2), pp. 255–268.

[42] Holena, M., and Demut, R., 2011. "Assessing the suitability of surrogate models in eolutionary optimization.". *In Information Technologies*, pp. 31–38.

[43] Mongillo, M., 2011. "Choosing basis functions and shape parameters for radial basis function methods". In SIAM Undergraduate Research Online.

[44] Mehmani, A., Chowdhury, S., Meinrenken, C. J., and Messac, A., 2017. "Concurrent surrogate model selection (cosmos): Optimizing model type, kernel function, and hyper-parameters". *Structural and Multidisciplinary Optimization.* (online).

[45] Ghassemi, P., Zhu, K., and Chowdhury, S., 2017. "Optimal Surrogate and Neural Network Modeling for Day-Ahead Forecasting of the Hourly Energy Consumption of University Buildings". In ASME 2017 International Design Engineering Technical Conferences (IDETC).

[46] Mehmani, A., Ghassemi, P., and Chowdhury, S., 2017. "Optimal Metamodeling to Interpret Activity Based Health Sensor Data". In ASME 2017 International Design Engineering Technical Conferences (IDETC).

[47] Mehmani, A., Chowdhury, S., and Messac, A., 2015. "Predictive quantification of surrogate model fidelity based on modal variations with sample density". *Structural and Multidisciplinary Optimization,* ***52***(2), pp. 353–373.

[48] Lophaven, S. N., Nielsen, H. B., and Sondergaard, J., 2002. Dace - a matlab kriging toolbox, version 2.0. Tech. Rep. IMM-REP-2002-12, Informatics and Mathematical Modelling Report, Technical University of Denmark.

[49] Chang, Chih-Chung, and Lin, C.-J., 2011. "LIBSVM: A library for support vector machines". *ACM Transactions on Intelligent Systems and Technology,* ***2***(3), pp. 27:1–27:27.